A Hardware and Simulation-based Framework for Design of SPAD Receivers in Scanning LiDAR Systems. International Image Sensor Workshop

A Hardware and Simulation-based Framework for Design of SPAD Receivers in Scanning LiDAR Systems

Sarrah M. Patanwala[1, 2], Hanning Mai[1], Alistair Gorman[1], Andreas Aßmann[2], Istvan Gyongy[1], Neale A. W. Dutton[2], Bruce R. Rae[2], and Robert K. Henderson [1]
[1]School of Engineering, Institute for Integrated Micro and Nano Systems, University of Edinburgh, UK
[2]STMicroelectronics Imaging Division, Edinburgh, UK
S.Patanwala@ed.ac.uk

***Abstract* – There are significant overheads involved in prototyping sensors for automotive Light Detection and Ranging (LiDAR) applications. We propose a framework that validates the performance of a Single Photon Avalanche Diode (SPAD) sensor in a controlled environment using a scanning LiDAR system. The results are further extrapolated to a simulation framework utilising synthetic datasets to investigate the merits of sensor architectures at longer distances in automotive LiDAR scenarios. We also present a high-throughput photon processing technique using a continuous sampling Time to Digital Converter (TDC) together with the Synchronous Summation Technique (SST); the performance of which is compared with previously demonstrated sensors. A SPAD pixel array interfaced to a FPGA provides the platform to implement the different design approaches for direct comparison.**

I. Introduction

Direct time-of-flight (dToF) sensors implemented with Single Photon Avalanche Diode (SPAD) are well suited for Light Detection and Ranging (LiDAR) applications, owing to their inherent ability to capture, with picosecond time resolution, individual photon arrival times. However, the prototyping of these sensors in an automotive environment can be expensive and challenging. It is therefore beneficial to employ analytical and simulation approaches to predict the performance of SPADs in the given application and verify the performance in controlled indoor conditions [1, 2].

We propose a framework that integrates the response of a SPAD array into synthetic datasets utilising realistic scenarios to evaluate the design parameters for sensors in long-range automotive applications. The modelling of sensor performance in this framework is validated with the aid of a scanning LiDAR setup and an accessible laser source that allows ranging over a few meters.

We further present a comparison of previously implemented dToF sensors alongside a high-throughput photon processing technique using a continuous sampling Time to Digital Converter (TDC) together with the Synchronous Summation Technique (SST) [3]. The comparison includes previously demonstrated sensor approaches that record one photon per laser emission cycle [4]; and multiple photons per frame accompanied with detection of spatial and temporal correlation of photons [5, 6]. The comparison aims to show the effect the different macro-pixel combining network and TDC design approaches can have on the ranging capabilities of the system.

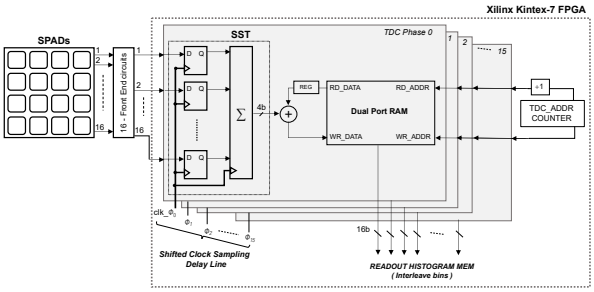

Fig. 1: Implementation of continuous sampling TDC and Synchronous Summation Technique (SST).

II. Sensor Description

The sensor utilises a macro-pixel of 4×4 SPADs with 15 μm pitch from a reconfigurable SPAD test chip [3]. The digital pulses corresponding to SPAD events, containing the time-of-arrival and SPAD dead time information, are readout to the FPGA. These pulses are then sampled using multi-phase shifted clock sampling approach [7]; with 16 phases of 250 MHz clock, providing a TDC resolution of 250 ps. The combining of pulses through SST gives a 4-bit output corresponding to the integral of photon counts. The retention of dead time information allows overlap of photon arrivals, thus incorporating coincidence between events.

The samples are saved using a dual-port RAM, with the read-accumulate operation of one location being carried out while writing into the previous location; 16 such memories (1 per clock phase) are instantiated. This helps accomplish zero dead time in the converter. The laser trigger resets the common address bus across the memories. The time-stamps accumulated over multiple laser cycles are readout from the memory as interleaved bins to create the histogram. The implementation is summarized in Fig. 1. The design approaches from [4, 5, 6] are reproduced on the FPGA, while maintaining an identical setup of the SPADs and TDC resolution. Thus, allowing direct comparison of the different configurations.

III. Experimental Setup

The scanning LiDAR optical setup is shown in Fig. 2. A pair of galvanometer mirrors are utilised for steering the laser beam in desired X-Y direction as well as collecting the photons reflected from the scene. The return photons are focused and aligned on to the SPAD

sensor with the help of a parabolic mirror and lens arrangement. The use of a parabolic mirror with through hole requires the surfaces in scene to either provide diffused reflections or specular reflections with an offset. The optical alignment carried out ensures minimum internal reflections on the SPAD pixels to be readout and processed on the FPGA. The histograms generated on FPGA are readout to MATLAB where a peak extraction algorithm using the Centre of Mass Method (CMM) is executed. The synchronisation of data acquisition and scan movement of the galvanometers is controlled through MATLAB. The controls and readout for the system are shown in Fig. 3.

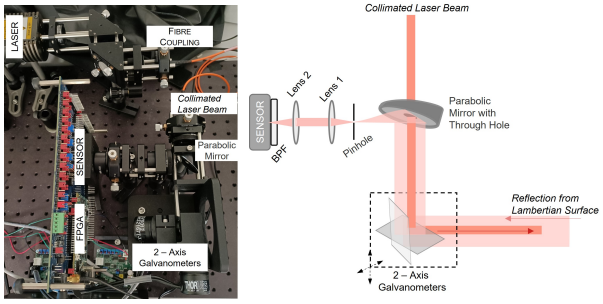

(a) (b)

Fig. 2: Scanning Optics - (a) Experimental Setup; (b) Block Diagram.

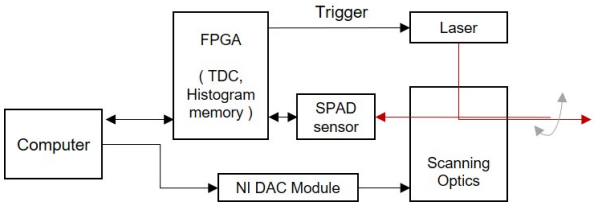

Fig. 3: Scanning LiDAR system controls.

IV. Simulation Framework

The performance of the scanning LiDAR system is calibrated and extrapolated to the simulation framework integrating synthetic datasets [8]. This aims to facilitate the comparison of sensor design approaches for long distance imaging. The dataset includes RGB, object segmentation and depth information for various automotive scenes; a sample scene is shown in Fig. 4a. A reflectivity map is assigned based on the material properties at NIR wavelength [9] with the aid of RGB and object segmentation information in the dataset. This, along with the input depth information, is processed through a camera transform as per desired scan resolution (Fig. 4b). The framework considers a linear scanning system that in return illuminates a column of macro-pixels at the sensor array simultaneously. The ground truth information at each angular position determines the incident photons on the corresponding macro-pixels, which are then processed through the sensor model.

The sensor model aims to reproduce the SPAD response using a Monte-Carlo simulator. The model

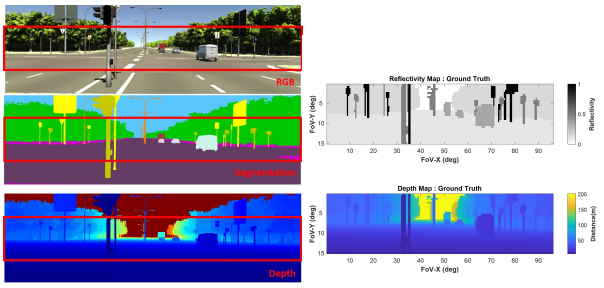

(a) (b)

Fig. 4: (a) Input information from synthetic data source [8]; (b) Applying camera transform to obtain ground truth for desired FOV and angular resolution.

generates incident photons with timing information related to background conditions and laser return from the target. The behaviour of passive quenched SPADs is replicated to generate the SPAD detection pulses; for the defined biasing conditions, photon detection probability, fill factor and dead time. The model also generates SPAD pulses occurring due to internal noise sources such as dark counts, afterpulsing and crosstalk between all the pixels active in the column. Dark counts occurring due to thermal carriers are generated with a uniform random distribution defined by the dark count rate (DCR). The afterpulses occur due to release of trapped charge carriers from a previous avalanche, and can cause a breakdown in the SPAD shortly after recovery. These afterpulses are generated based on afterpulsing probability (P_{ap}) and lifetime of the trapped carrier for the given SPADs. The false triggers from crosstalk occur due to optical or electrical diffused carriers from a neighbouring triggered SPAD. These pulses are generated considering the crosstalk probability (P_{ct}) and relative locations of the SPADs.

Design Parameter		Value
Wavelength	λ	840 nm
Field of View	$FoV_x \times FoV_y$	96°× 15°
Angular resolution	$\theta_x \times \theta_y$	0.5°× 0.5°
Optical filter passband		±10 nm
Frame rate	f_{int}	30 fps
Laser pulse width	t_{pulse}	4 ns
Avg. laser power	P_{Tx}	30 mW
Pulse repetition rate	PRR	750 kHz

TABLE I: LiDAR system parameters.

SPAD Parameters		Value
Photon detection probability	PDE	5%
SPAD pitch		15 μm
Fill Factor	FF	60.5%
Dead time	t_d	10 ns
Dark Count rate	DCR	65 cps
After-pulsing probability	P_{ap}	0.2%
Crosstalk probability	P_{ct} (Horiz.)	3.021%
	P_{ct} (Vert.)	1.087%
	P_{ct} (Diag.)	0.725%

TABLE II: SPAD parameters.

The generated SPAD events are processed using the respective combining technique and the TDC design

approach. Tables I and II outline the LiDAR system parameters and measured SPAD characteristics used for the modelling. The histograms are accumulated by simulating the response for 100 laser cycles at each position in the scene to achieve a frame rate of 30 fps. These histograms are then processed through CMM to estimate the depth information.

V. Results

A. Scanning LiDAR measurements

The laser used in the experimental setup has a wavelength of 840 nm, pulse width set to 4 ns and repetition rate of 12 MHz. It provides an average output power of 5 mW. In Fig. 5, the measured distance and its precision is compared for each of the TDC implementations. The measured distance is the mean value calculated from a set of 500 measurements and is plotted as function of actual distance for a white target and a black target, with reflectivity of 99% and 10% respectively. Similarly, precision is presented as the standard deviation in relation to actual distance. The exposure time for each measurement is 840 μs, i.e histograms are generated with 10000 laser repetition cycles.

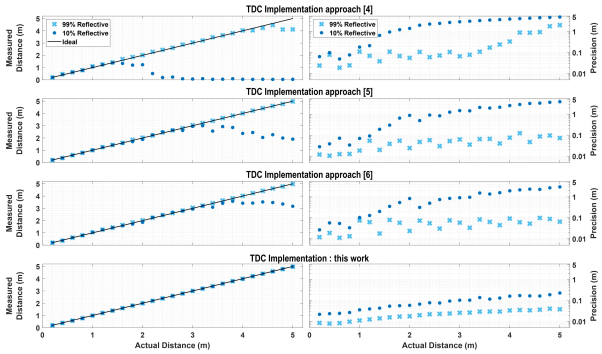

Fig. 5: Measured distance plots mean value calculated from 500 measurements as function of actual distance for white target (99% reflective) and black target (10% reflective) for each of the TDC implementation approach. Precision is plotted as standard deviation within set of measurements with respect to the actual distance. These measurements were made in dark, to aid calibration of simulation framework.

Fig. 6 shows the objects placed in the field-of-view (FoV) of the scanning system. A Thorlabs CMOS camera is used to calibrate the reflectivity of objects in the scene with respect to the standard 99% Lambertian reference. The ambient lighting in the room is measured as 160 μW/cm^2. The laser settings are kept the same as before. Due to system limitations only a single point scan is implemented. Fig. 7 shows scanned measurement results for the different design approaches. It can be observed that the other techniques are unable to detect objects with low reflectivity even in close proximity. The implementation presented in this work shows immunity to object reflectivity and is able to accurately capture the scene information.

The data from the measurements described above is used to calibrate the performance and efficiency of the

Class	Refl.
{1}	0.99
{2}	0.96
{3}	0.85
{4}	0.60
{5}	0.50
{6}	0.40
{7}	0.20
{8}	0.15
{9}	0.10
{10}	0.05

Fig. 6: Photograph of objects with varied reflectivity placed in the FoV of scanning system.

scanning system. Optical simulations using Zemax software are also used to verify the ratios between power transmitted from the system to power received back on to the sensor. The power ratios obtained are scaled as a function of inverse square law for Lambertian targets at further distances.

B. Synthetic 3D data simulations

The sensor response is simulated with the system parameters outlined in Table I and SPAD characteristics from Table II, for synthetic data scene shown in Fig. 4. The system efficiency and optical response is determined by the calibration of scanning LiDAR experimental setup. Moreover, the maximum ranging distance in simulations is set to an expected realistic automotive LiDAR range of 200 m. The assumed linear scan illuminates a column of 30 macro-pixels in the sensor. The ambient level is set to 1.96 W/m^2, equivalent to 10 klux outdoor daylight conditions.

Fig. 8 shows the depth maps and the point clouds superimposed with intensity information, for the different sensor implementations. For visual clarity, the depth estimates are only shown if they fall within $\pm$15 cm of the ground truth. The implementation from [4] demonstrates poor performance due to converter pile-up in high ambient conditions, as it is based on the TDC triggering at the arrival of first photon. The response improves slightly for implementations [5, 6], as they record multiple events per laser cycle. However, they are still unable to detect objects with low reflectivity and at further distances. The continuous sampling approach and ability to record data from multiple concurrent events using SST, provides immunity to pile-up conditions in converter occurring either due to high ambient or false triggers from internal noise sources in the SPAD sensor. This robustness in the design allows the sensor to range for longer distances and is demonstrated in the simulated response where the implementation presented in this work is able to correctly reproduce the scene information.

VI. Conclusion

The different photon processing techniques in the sensor have a direct effect on the ranging capabilities of the LiDAR system. This is demonstrated in both measured data at short-range and simulated response for long-range. The implementation of continuous sampling TDC and Synchronous Summation Technique (SST) outperforms all other techniques, and proves

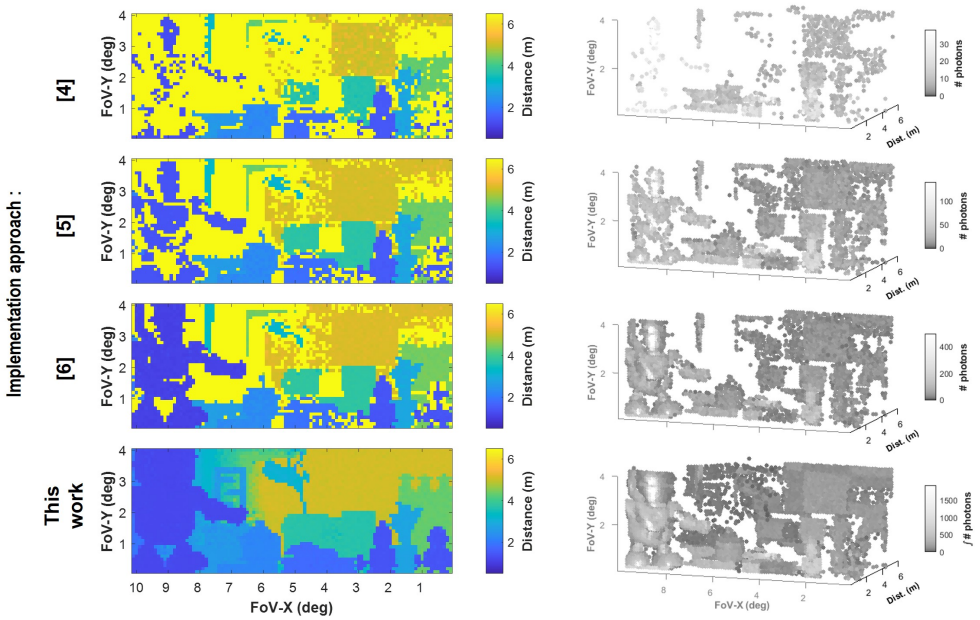

Fig. 7: Measured 3D imaging data using scanning LiDAR experimental setup, with ambient room lighting of 160 μW/cm^2. The rows show results for the different TDC implementation approaches, alongside point clouds superimposed with intensity data. Objects in scene are located between 1-5 m from the scanning system.

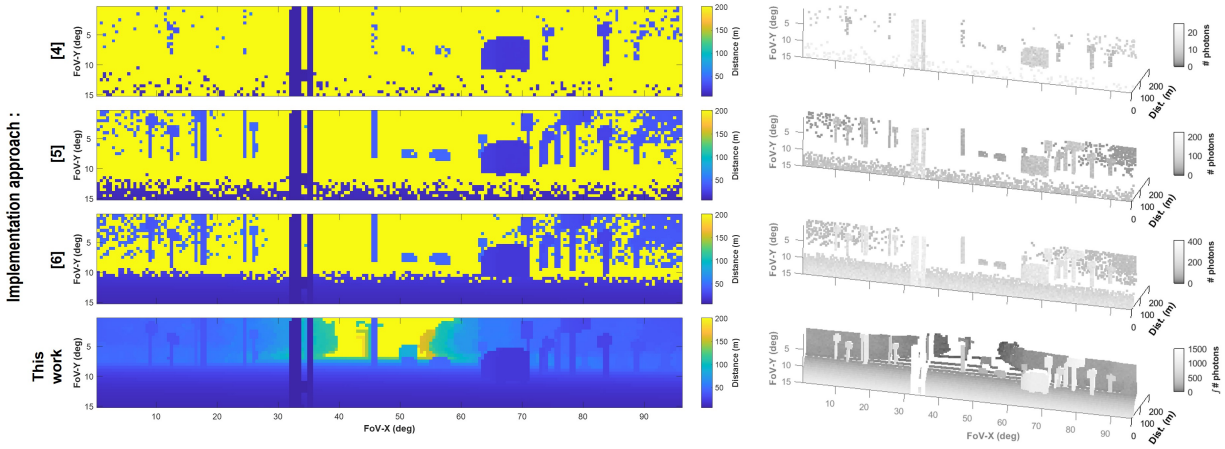

Fig. 8: Simulated sensor response demonstrated as 3D images and point cloud data overlaid with intensity, for synthetic data set shown in Fig. 4, with ambient level set to 10 klux imitating outdoor daylight conditions. Incorrect depth estimates are set to 200 m for improved visual contrast.

effective for long-range automotive LiDAR. Leveraging of synthetic datasets to evaluate the sensor response at longer distances, helps overcome limitations and challenges of prototyping in an automotive environment.

References

[1] A. Tontini *et al.*, "Numerical Model of SPAD-Based Direct Time-of-Flight Flash LIDAR CMOS Image Sensors," *Sensors*, vol. 20, no. 18, p. 5203, 2020.

[2] P. Padmanabhan *et al.*, "Modeling and analysis of a direct time-of-flight sensor architecture for LiDAR applications," *Sensors*, vol. 19, no. 24, p. 5464, 2019.

[3] S. M. Patanwala *et al.*, "A reconfigurable 40 nm CMOS SPAD array for LiDAR receiver validation," in *Proc. Int. Image Sensor Workshop*, 2019, pp. 1–4.

[4] C. Niclass *et al.*, "A 128x128 Single-Photon Image Sensor With Column-Level 10-Bit Time-to-Digital Converter Array," *IEEE Journal of Solid-State Circuits*, vol. 43, no. 12, pp. 2977–2989, 2008.

[5] C. Niclass *et al.*, "A 100m-range 10-frame/s 340x96-pixel Time-of-Flight depth sensor in 0.18μm CMOS," *IEEE Journal of Solid-State Circuits*, vol. 48, no. 2, pp. 559–572, 2012.

[6] S. W. Hutchings *et al.*, "A reconfigurable 3-D-stacked SPAD imager with in-pixel histogramming for flash LIDAR or high-speed time-of-flight imaging," *IEEE Journal of Solid-State Circuits*, vol. 54, no. 11, pp. 2947–2956, 2019.

[7] M. Büchele *et al.*, "The GANDALF 128-Channel Time-to-Digital Converter," *Physics Procedia*, vol. 37, pp. 1827–1834, 2012.

[8] A. Gaidon *et al.*, "Virtual worlds as proxy for multi-object tracking analysis," in *Proceedings of the IEEE conference on computer vision and pattern recognition*, 2016, pp. 4340–4349.

[9] A. M. Baldridge *et al.*, "The ASTER spectral library version 2.0," *Remote Sensing of Environment*, vol. 113, no. 4, pp. 711–715, 2009.